Multi-pulse edge-localized states on quantum graphs

Adilbek Kairzhan[1] · **Dmitry E. Pelinovsky**[2]

Abstract
We construct the edge-localized stationary states of the nonlinear Schrödinger equation on a general quantum graph in the limit of large mass. Compared to the previous works, we include arbitrary multi-pulse positive states which approach asymptotically a composition of N solitons, each sitting on a bounded (pendant, looping, or internal) edge. We give sufficient conditions on the edge lengths of the graph under which such states exist in the limit of large mass. In addition, we compute the precise Morse index (the number of negative eigenvalues in the corresponding linearized operator) for these multi-pulse states. If N solitons of the edge-localized state reside on the pendant and looping edges, we prove that the Morse index is exactly N. The technical novelty of this work is achieved by avoiding elliptic functions (and related exponentially small scalings) and closing the existence arguments in terms of the Dirichlet-to-Neumann maps for relevant parts of the given graph. We illustrate the general results with three examples of the flower, dumbbell, and single-interval graphs.

1 Introduction

We address standing waves of the focusing NLS (nonlinear Schrödinger) equation posed on a quantum graph $\Gamma = \{\mathcal{E}, \mathcal{V}\}$, where $\mathcal{E}$ is the set of edges and $\mathcal{V}$ is the set of vertices (see [22,24] for review). The evolution system can be written in the normalized form:

$$i\Psi_t + \Delta\Psi + 2|\Psi|^2\Psi = 0, \tag{1.1}$$

✉ Dmitry E. Pelinovsky
dmpeli@math.mcmaster.ca

Adilbek Kairzhan
kairzhan@math.toronto.edu

1   Department of Mathematics, University of Toronto, Toronto, ON, Canada

2   Department of Mathematics, McMaster University, Hamilton, ON L8S 4K1, Canada

Birkhäuser

where the Laplacian Δ and the nonlinear term are defined componentwise on edges $\mathcal{E}$ subject to proper boundary conditions on the vertices $\mathcal{V}$ (see [5,11] for introduction to linear differential equations on quantum graphs).

The quantum graph $\Gamma = \{\mathcal{E}, \mathcal{V}\}$ is assumed to consist of a finite number $|\mathcal{E}|$ of bounded and unbounded edges. Enumerating every edge in Γ uniquely gives the set $\mathcal{E} = \{e_1, e_2, \ldots, e_{|\mathcal{E}|}\}$. The function Ψ on Γ can be represented as a vector with $|\mathcal{E}|$ components,

$$\Psi = \{\psi_1, \psi_2, \ldots, \psi_{|\mathcal{E}|}\}, \tag{1.2}$$

where ψ_j is defined on the edge e_j only. The function Ψ can be defined in the Hilbert space of square-integrable functions $L^2(\Gamma) = \bigoplus_{e\in\mathcal{E}} L^2(e)$.

Weak (resp. strong) solutions of the NLS time flow (1.1) are well defined in the L^2-based Sobolev spaces $H^1(\Gamma)$ (resp. $H^2(\Gamma)$), where $H^{1,2}(\Gamma) = \bigoplus_{e\in\mathcal{E}} H^{1,2}(e)$, provided the boundary conditions on $\mathcal{V}$ are symmetric. Since $|\mathcal{E}| < \infty$, the NLS time flow (1.1) is essentially the evolution problem in one spatial dimension, which is globally well-posed both in $H^1(\Gamma)$ and $H^2(\Gamma)$ due to the cubic (L^2-subcritical) nonlinearity.

We consider *the natural Neumann–Kirchhoff (NK) boundary conditions* at each vertex $v \in \mathcal{V}$ given by

$$\begin{cases} \Psi \text{ is continuous on } \Gamma, \\ \sum_{e\sim v} \partial\Psi(v) = 0 \text{ for every vertex } v \in \mathcal{V}, \end{cases} \tag{1.3}$$

where the derivatives ∂ are directed away from the vertex $v \in \mathcal{V}$ and $e \sim v$ denotes the edges $e \in \mathcal{E}$ adjacent to the vertex $v \in \mathcal{V}$.

Consistent with the boundary conditions (1.3), weak solutions of the NLS equation (1.1) are defined in the energy space $H_C^1(\Gamma) := H^1(\Gamma) \cap C^0(\Gamma)$, where $C^0(\Gamma)$ denotes the space of functions continuous on all edges in $\mathcal{E}$ and across all vertex points in $\mathcal{V}$. These weak solutions conserve the energy and mass functionals given respectively by

$$E(\Psi) = \|\nabla\Psi\|_{L^2(\Gamma)}^2 - \|\Psi\|_{L^4(\Gamma)}^4, \quad Q(\Psi) = \|\Psi\|_{L^2(\Gamma)}^2. \tag{1.4}$$

Standing waves of the NLS equation (1.1) are given by the solutions of the form $\Psi(t, x) = \Phi(x)e^{-i\omega t}$, where $\Phi \in H_C^1(\Gamma)$ is a weak solution of the stationary NLS equation

$$\omega\Phi = -\Delta\Phi - 2|\Phi|^2\Phi, \tag{1.5}$$

for a given $\omega \in \mathbb{R}$. By bootstrapping arguments, every weak solution of the stationary NLS equation (1.5) is also a strong solution satisfying the natural NK conditions (1.3). Hence, we can use the vector representation $\Phi = (\phi_1, \phi_2, \ldots, \phi_{|\mathcal{E}|})$ and rewrite the stationary NLS equation (1.5) on every edge e_j in $\mathcal{E}$ as a collection of differential equations:

$$\omega\phi_j(x) = -\phi_j''(x) - 2|\phi_j(x)|^2\phi_j(x), \quad x \in e_j, \tag{1.6}$$

which satisfy the boundary conditions (1.3) on every vertex $v \in \mathcal{V}$. We write $\Phi \in H_{\mathrm{NK}}^2(\Gamma)$ if $\Phi \in H^2(\Gamma)$ satisfies the NK conditions (1.3). Only *real-valued* solutions of the stationary NLS equation are considered but we write the modulus sign for easy generalizations.
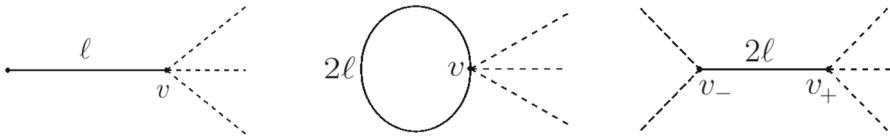
Fig. 1 Schematic illustration of a pendant edge (left), a looping edge (middle), and an internal edge (right)

Among all possible real-valued solutions of the stationary NLS equation (1.5), we are particularly interested in the *positive edge-localized states* which satisfy the following conditions:

- $\Phi(x) > 0$ for every $x \in \Gamma$;
- on each bounded edge $e_j \in \mathcal{E}$, there is at most one local critical point of ϕ_j (either maximum or minimum) inside the edge;
- on each unbounded edge $e_j \in \mathcal{E}$, the function ϕ_j is monotonically decreasing and has exponential decay to 0 at infinity.

Depending on the topological properties of the quantum graph Γ, the positive edge-localized states could become *the ground state*, the state of the least energy $E(\Psi)$ at fixed mass $Q(\Psi)$ [1–3].

Although the set of conditions on Φ seems to be restrictive, the positive edge-localized states exist *in the limit of large mass* [4,6,10,19]. This limit for large $\mu = Q(\Phi)$ can be recast as the limit of large negative ω in the stationary NLS equation (1.5) for the cubic (L^2-subcritical) nonlinearity. Existence of such edge-localized states was confirmed analytically and/or numerically for the tadpole graph [2,8,9,23,25], the dumbbell graph [14,21], and the flower graph [17]. The importance of the positive edge-localized states is motivated by their (possible) orbital stability in the NLS time flow.

Bounded edges of $\mathcal{E}$ are divided into pendant, looping, and internal edges according to the following classification (see illustrations on Fig. 1):

- *A pendant edge* of length ℓ is associated with the segment $[0, \ell]$, where the left end is isolated from the rest of Γ subject to the Neumann boundary condition and the right end is connected with the rest of Γ at a vertex v.
- *A looping edge* of length 2ℓ is associated with the segment $[-\ell, \ell]$, where both ends at connected to the rest of Γ at a single vertex v, hence contributing twice to the derivative condition in (1.3).
- *An internal edge* of length 2ℓ is associated with the segment $[-\ell, \ell]$, where different ends at connected to the rest of Γ at two different vertices v_- and v_+.

Each unbounded edge is associated with the half-line $[0, \infty)$. The edge-localized states considered in [6] are formed by a single large-amplitude component ϕ_e on a fixed looping or internal edge e of length 2ℓ such that ϕ_e has a single local maximum inside e, monotone from its maximum to the vertices of e, and concentrated on e in the following sense

$$\frac{\|\Phi\|_{L^2(e)}}{\|\Phi\|_{L^2(\Gamma)}} \geq 1 - Ce^{-2\epsilon\ell}, \tag{1.7}$$
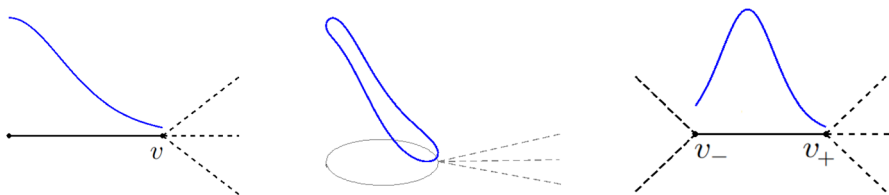
Fig. 2 Schematic illustration of edge-localized states on a pendant (left), a looping edge (middle), and an internal edge (right)

where $\epsilon := \sqrt{|\omega|}$ is a large parameter and the constant C is independent of ϵ. Moreover, Φ has no internal maxima on the remainder of graph $\Gamma\backslash\{e\}$. The edge-localized state on the pendant edge e is formed similarly except that ϕ_e has a single local maximum at the terminal vertex. The edge-localized states considered in [6] are illustrated on Fig. 2.

The construction of the edge-localized states in [6] relies on the properties of elliptic functions and on careful rescaling of exponentially small terms for the elliptic modulus. In addition, the states of the least energy at fixed mass were analyzed in [6] by comparing the exponentially small terms in the expansion of $\mu := Q(\Phi)$ in $\epsilon := \sqrt{|\omega|}$.

A similar result on the edge-localized states in the large-mass limit was obtained independently in [4] using variational methods (for unbounded graphs only). Since the edge-localized states were identified in [4] as local energy minimizers in the restricted space of functions in $H_C^1(\Gamma)$ that attain their maximum on a given edge e, the Morse index for such states is exactly one, where *the Morse index* is the number of negative eigenvalues of the linearized operator $\mathcal{L} : H_{NK}^2(\Gamma) \subset L^2(\Gamma) \to L^2(\Gamma)$ given by

$$\mathcal{L} = -\Delta - \omega - 6|\Phi|^2. \tag{1.8}$$

If $\omega < 0$, the graph Γ is unbounded, and Φ is bounded and decays to 0 at infinity exponentially fast, then the linearized operator $\mathcal{L}$ is self-adjoint and the absolutely continuous part of the spectrum is strictly positive and bounded away from zero by $|\omega|$ by Weyl's theorem on essential spectrum. Therefore, the Morse index is well-defined as the finite number of negative eigenvalues of $\mathcal{L}$ accounting for their finite multiplicity. We denote this number by $n(\mathcal{L})$. We also denote the multiplicity of the zero eigenvalue of $\mathcal{L}$ by $z(\mathcal{L})$.

If the graph Γ is bounded, then the spectrum of $\mathcal{L}$ is purely discrete and the numbers $n(\mathcal{L})$ and $z(\mathcal{L})$ are again well-defined since $\mathcal{L}$ is bounded from below.

Additional results related to the edge-localized states in the limit of large energy were obtained in [10], where bounded graphs with the pendant edges were considered and convergence of the edge-localized states to the half-solitons was proven. Multi-pulse states were also studied in [10], all pulses localize at the terminal vertices. Edge-localized states were considered in [19] by recasting the existence problem to the semi-classical limit of an elliptic problem. It was proven in [19] that the location of the edge-localized state with a single maximum as the state of the least energy at fixed mass is determined by the longest pendant edge of a bounded graph or the longest

internal edge if no pendant and looping edges are present. These results are included in more general results obtained in [6].

The main result of this work concerns the construction of the multi-pulse edge-localized states in the limit of large mass (large negative ω). As $\omega \to -\infty$, the multi-pulse states approach asymptotically a composition of N solitons, each sitting on a bounded (pendant, looping, or internal) edge. The edges of the graph, where the multi-pulse state is localized, must satisfy the following non-degeneracy assumptions.

Assumption 1 Let $\mathcal{E}_N := \{e_1, e_2, \ldots, e_N\}$ be the set of N edges connected to the remainder graph $\Gamma \backslash \mathcal{E}_N$ at $|B|$ boundary vertices $\mathcal{V}_B = \{v_1, v_2, \ldots, v_{|B|}\}$. Let $\ell_{\min}$ be the length of the shortest edge in $\Gamma \backslash \mathcal{E}_N$ and $\ell_{j,\min}$ be the minimal half-length of the looping and internal edges or the minimal length of the pendant edges adjacent to the boundary vertex $v_j \in \mathcal{V}_B$ from $\mathcal{E}_N$, $1 \leq j \leq |B|$. The edge lengths must satisfy the constraints:

$$\max_{1 \leq j \leq |B|} \ell_{j,\min} - \min_{1 \leq j \leq |B|} \ell_{j,\min} < \ell_{\min} \tag{1.9}$$

and

$$\max_{1 \leq j \leq |B|} \ell_{j,\min} < 3 \min_{1 \leq j \leq |B|} \ell_{j,\min}. \tag{1.10}$$

Assumption 2 Each internal edge in $\mathcal{E}_N$ has no common vertices with other internal edges in $\mathcal{E}_N$ and its half-length is strictly minimal among the half-lengths of the looping edges and the lengths of the pendant edges in $\mathcal{E}_N$ adjacent to its two vertices.

Remark 1 In the definition of the edge lengths, we assume that each vertex has degree 3 or higher, except for the terminal vertices of the pendant edges which have degree 1. In other words, we do not allow dummy vertices of degree 2 in the graph Γ.

Remark 2 If $N = 1$, both Assumptions 1 and 2 are satisfied trivially. If $|B| = 0$ or $|B| = 1$ or $|B| \geq 2$ and all $\ell_{j,\min}$ are equal, Assumption 1 is satisfied.

The following theorem gives the existence result.

Theorem 1 Let $\Gamma = \{\mathcal{E}, \mathcal{V}\}$ be a graph with finitely many edges and satisfying NK conditions at its vertices. For any N edges $\mathcal{E}_N := \{e_1, e_2, \ldots, e_N\}$ of finite lengths satisfying Assumptions 1 and 2 and for large enough $\epsilon := \sqrt{-\omega}$ there exists a positive edge-localized state Φ with the following properties:

(1) $\Phi|_{e_j}$ has a single local maximum and is monotone from its maximum to the end vertices of $e_j \in \mathcal{E}_N$, for $1 \leq j \leq N$;
(2) Φ has no internal maxima on the remainder of the graph $\Gamma \backslash \mathcal{E}_N$;
(3) Φ is concentrated on $\mathcal{E}_N$ in the following sense

$$\frac{\|\Phi\|_{L^2(\Gamma \backslash \mathcal{E}_N)}}{\|\Phi\|_{L^2(\mathcal{E}_N)}} \leq C e^{-\epsilon \ell_N}, \tag{1.11}$$

where the constant C is independent of ϵ and $\ell_N = \min\{\ell_{1,\min}, \ell_{2,\min}, \ldots, \ell_{|B|,\min}\}$.

Remark 3 For the pendant edge $e_j \in \mathcal{E}_N$, the maximum of $\Phi|_{e_j}$ occurs at the left end with the Neumann boundary conditions. For the looping edge $e_j \in \mathcal{E}_N$, the maximum of $\Phi|_{e_j}$ occurs exactly at the middle point. For the internal edge $e_j \in \mathcal{E}_N$, the maximum of $\Phi|_{e_j}$ is generally shifted from the middle point. Assumption 2 allows us to control the shift of the maximum of $\Phi|_{e_j}$ on the internal edge. See Fig. 2 for illustration of edge-localized states.

Remark 4 Condition (1.11) is equivalent to (1.7) in the case $N = 1$ and $\mathcal{E}_N = \{e\}$. Indeed, it follows from (1.11) with $\ell_{N=1} = \ell$ that

$$\|\Phi\|_{L^2(\Gamma)}^2 = \|\Phi\|_{L^2(e)}^2 + \|\Phi\|_{L^2(\Gamma \setminus \{e\})}^2 \leq (1 + C^2 e^{-2\epsilon\ell})\|\Phi\|_{L^2(e)}^2, \qquad (1.12)$$

which yields (1.7). It follows from Theorems 3.1, 3.3, and 3.5 in [6] that

$$|\|\Phi\|_{L^2(e)}^2 - \epsilon| \leq C\epsilon^2 e^{-2\epsilon\ell} \qquad (1.13)$$

for the pendant edge and

$$|\|\Phi\|_{L^2(e)}^2 - 2\epsilon| \leq C\epsilon^2 e^{-2\epsilon\ell} \qquad (1.14)$$

for the looping and internal edges, where the constant C is independent of ϵ. In the case of N edges, we have

$$\|\Phi\|_{L^2(\mathcal{E}_N)}^2 = \sum_{j=1}^N \|\Phi\|_{L^2(e_j)}^2 \qquad (1.15)$$

with similar estimates for $\|\Phi\|_{L^2(e_j)}^2$, where $e_j \in \mathcal{E}_N$.

Remark 5 Compared to the work in [6], we do not use elliptic functions and exponentially small scalings, which makes our results more general and the proofs simpler. We partition the graph Γ into $\mathcal{E}_N$ and $\Gamma \setminus \mathcal{E}_N$ and reduce the existence problem to a system of equations for Dirichlet data on the boundary vertices in $\mathcal{V}_B$. Then, we show that all these equations can be solved independently of each other under the constraints (1.9) and (1.10) on the lengths of edges in Assumption 1, which provide compatability of asymptotic solutions for large ϵ.

Our second main result is the precise characterization of the Morse index $n(\mathcal{L})$ and the degeneracy index $z(\mathcal{L})$ of the multi-pulse edge-localized states in the limit of large mass (large negative ω). This characterization was not provided in [6] even in the case of $N = 1$. The following theorem gives the result when the set $\mathcal{E}_N$ does not include internal edges.

Theorem 2 *Let Φ be the positive N-pulse edge-localized state of Theorem 1 for large enough ϵ and assume that the set $\mathcal{E}_N$ contains only pendant and looping edges. Then, $n(\mathcal{L}) = N$ and $z(\mathcal{L}) = 0$, where $\mathcal{L}$ is the linearized operator in (1.8).*

Remark 6 To obtain the exact count of the Morse index and the multiplicity of the zero eigenvalue of $\mathcal{L}$, we use a homotopy argument relating the non-positive spectra of the operators $\mathcal{L} : H^2_{NK}(\Gamma) \subset L^2(\Gamma) \to L^2(\Gamma)$ and $\mathcal{L}_D : H^2_D(\Gamma) \subset L^2(\Gamma) \to L^2(\Gamma)$ where $\mathcal{L}_D$ has the same differential representation as $\mathcal{L}$ and $H^2_D(\Gamma)$ differs from $H^2_{NK}(\Gamma)$ by the Dirichlet conditions at the boundary vertices in $\mathcal{V}_B$ instead of the NK conditions. The technique resembles the surgery principle widely used in the spectral analysis of differential operators on graphs [7,20].

Remark 7 If an internal edge is present in the set $\mathcal{E}_N$, then the explicit count of the Morse index in Theorem 2 is no longer applicable, as shown in Example 3. Therefore, characterization of the Morse index and the multiplicity of the zero eigenvalue of $\mathcal{L}$ is still an open problem in the case of multi-pulse states localized on internal edges.

Remark 8 The implication of Theorem 2 to the time evolution of perturbations to the positive N-pulse edge-localized states of Theorem 1 is that these states are orbitally unstable under the NLS time flow (1.1) if $N \geq 2$. This follows from an easy application of the main results of [15] and [26]. In agreement with the variational characterization of the single-pulse states on unbounded graphs Γ in [4], the positive edge-localized states with $N = 1$ are orbitally stable. This follows via the standard orbital stability theory [16] from the monotonicity of the mapping

$$\epsilon \mapsto \|\Phi\|^2_{L^2(\mathcal{E}_N)} \tag{1.16}$$

for large ϵ and the exponential smallness of $\|\Phi\|_{L^2(\Gamma \setminus \mathcal{E}_N)}$ due to the bound (1.11), the decomposition (1.15) and the bounds (1.13) and (1.14). Note that it was proven in [6] that the mapping (1.16) is C^1.

Remark 9 Multi-pulse states with $N \geq 2$ cannot be the ground state because $n(\mathcal{L}) \geq 2$. It is still unclear (see discussion in [6]) if the ground state can only be realized among the single-pulse edge-localized states of Fig. 2 in the large-mass limit.

The paper is organized as follows. Section 2 reviews preliminary results from [6] and [17]. Sections 3 and 4 give the proof of Theorems 1 and 2 respectively. Section 5 contains examples of flower, dumbbell, and single-interval graphs where Theorems 1 and 2 are applicable and discuss counter-examples when assumptions of Theorem 2 are violated. Section 6 concludes the paper with a summary and open directions.

2 Preliminary results

Since $\epsilon := \sqrt{-\omega}$ is considered to be large, we rescale the stationary NLS equation (1.5) with the transformation $\Phi(x) = \epsilon U(\epsilon x)$, $x \in \Gamma$. As a result, the graph $\Gamma = \{\mathcal{E}, \mathcal{V}\}$ is transformed to the ϵ-scaled graph $\Gamma_\epsilon = \{\mathcal{E}_\epsilon, \mathcal{V}\}$ for which every bounded edge $e \in \mathcal{E}$ of length ℓ_e transforms to the edge $e_\epsilon \in \mathcal{E}_\epsilon$ of length $\epsilon \ell_e$ but the unbounded edge $e \in \mathcal{E}$ remains the same as $e \in \mathcal{E}_\epsilon$. The stationary NLS equation (1.5) is rewritten in the parameter-free form

$$(1 - \Delta)U - 2|U|^2 U = 0. \tag{2.1}$$

Writing $U = (u_1, u_2, \ldots, u_{|\mathcal{E}|})$ gives a collection of differential equations

$$-u_j''(z) + u_j(z) - 2|u_j(z)|^2 u_j(z) = 0, \quad z \in e_{j,\epsilon}, \tag{2.2}$$

subject to the boundary conditions (1.3) at vertices $v \in \mathcal{V}$.

We select N edges $\mathcal{E}_N := \{e_1, e_2, \ldots, e_N\}$ with $N \leq |\mathcal{E}|$ in the original graph Γ and partition the graph into two parts $\mathcal{E}_N$ and $\Gamma \backslash \mathcal{E}_N$. The two graphs intersect at the vertices in the set $\mathcal{V}_B := \{v_1, v_2, \ldots, v_{|B|}\}$, which are referred to as *boundary vertices*. After rescaling of Γ to Γ_ϵ, we obtain $\mathcal{E}_{N,\epsilon}$ and $\Gamma_\epsilon \backslash \mathcal{E}_{N,\epsilon}$.

We introduce the Dirichlet data on the boundary vertices $\mathbf{p} = (p_1, p_2, \ldots, p_{|B|})$ and the Neumann data $\mathbf{q} = (q_1, q_2, \ldots, q_{|B|})$ for the graph $\Gamma_\epsilon \backslash \mathcal{E}_{N,\epsilon}$ with

$$p_j := u_{e \sim v_j}(v_j), \quad q_j := \sum_{e \sim v_j} \partial u_e(v_j), \quad v_j \in \mathcal{V}_B, \tag{2.3}$$

where the derivatives ∂ are directed away from $\Gamma_\epsilon \backslash \mathcal{E}_{N,\epsilon}$ and $e \sim v_j$ lists all edges $e \in \Gamma_\epsilon \backslash \mathcal{E}_{N,\epsilon}$ incident to the vertex v_j. We are looking for solutions of the differential equations (2.2) such that

$$\sup_{z \in e_{j,\epsilon}} |u_j(z)| < \frac{1}{\sqrt{2}}, \quad e_{j,\epsilon} \in \Gamma_\epsilon \backslash \mathcal{E}_{N,\epsilon}, \tag{2.4}$$

and

$$\sup_{z \in e_{j,\epsilon}} |u_j(z)| > \frac{1}{\sqrt{2}}, \quad e_{j,\epsilon} \in \mathcal{E}_{N,\epsilon} \tag{2.5}$$

where $\frac{1}{\sqrt{2}}$ is the constant solution of the differential equations in (2.2).

The following two lemmas were proven in [6] (Theorem 2.9 and Lemma 2.12).

Lemma 1 *There exist $C_0 > 0$, $p_0 > 0$, and $\epsilon_0 > 0$ such that for every $\mathbf{p}$ with $\|\mathbf{p}\| < p_0$ and every $\epsilon > \epsilon_0$, there exists a solution $U \in H_{\mathrm{NK}}^2(\Gamma_\epsilon \backslash \mathcal{E}_{N,\epsilon})$ to the stationary NLS equation (2.1) on $\Gamma_\epsilon \backslash \mathcal{E}_{N,\epsilon}$ subject to the Dirichlet data on $\mathcal{V}_B$ which is unique among functions satisfying (2.4). The solution satisfies the estimate*

$$\|U\|_{H^2(\Gamma_\epsilon \backslash \mathcal{E}_{N,\epsilon})} \leq C_0 \|\mathbf{p}\|, \tag{2.6}$$

while its Neumann data satisfies

$$|q_j - D_j p_j| \leq C_0 \left(\|\mathbf{p}\| e^{-\epsilon \ell_{\min}} + \|\mathbf{p}\|^3 \right), \quad 1 \leq j \leq |B|, \tag{2.7}$$

where D_j is the degree of the j-th boundary vertex in $\Gamma_\epsilon \backslash \mathcal{E}_{N,\epsilon}$ and $\ell_{\min}$ is the length of the shortest edge in $\Gamma \backslash \mathcal{E}_N$. Furthermore, if $p_j \geq 0$ for every j, then $U(z) \geq 0$ for all $z \in \Gamma_\epsilon \backslash \mathcal{E}_{N,\epsilon}$ and U has no internal local maxima in $\Gamma_\epsilon \backslash \mathcal{E}_{N,\epsilon}$.

Lemma 2 *There exist $C_0 > 0$, $p_0 > 0$, and $\epsilon_0 > 0$ such that for every $p \in (0, p_0)$ and every $\epsilon > \epsilon_0$, there exists a real solution $u \in H^2(0, \epsilon \ell)$ to the differential equation*

$-u'' + u - 2u^3 = 0$ satisfying $u'(0) = 0$ and $u(\epsilon\ell) = p$, which is unique among positive and decreasing functions satisfying (2.5). The solution satisfies $u'(\epsilon\ell) < 0$ and

$$\left| u'(\epsilon\ell) - u(\epsilon\ell) + 4e^{-\epsilon\ell} \right| \leq C_0 \epsilon e^{-3\epsilon\ell}. \tag{2.8}$$

Remark 10 The C^1 property of Neumann data $\mathbf{q}$ and $u'(\epsilon\ell)$ with respect to parameter ϵ and Dirichlet data $\mathbf{p}$ and $u(\epsilon\ell) = p$ in Lemmas 1 and 2 respectively was established in [6] with similar exponentially small estimates. We will not write this property explicitly but will use the C^1 property in the application of the implicit function theorem.

Remark 11 The solution $u(z)$ in Lemma 2 was represented by elliptic functions and its dependence on the elliptic modulus was also studied in Lemma 2.12 of [6]. This information is not used in the present work.

For the solution $u \in H^2(0, \epsilon\ell)$ to the differential equation $-u'' + u - 2u^3 = 0$ in Lemma 2, we write the boundary conditions as

$$p_+ := u(0), \quad 0 = u'(0), \quad p := u(\epsilon\ell), \quad q := -u'(\epsilon\ell), \tag{2.9}$$

where $p_+ \in (p, 1)$, $p > 0$, and $q > 0$. Denoting $v(z) := u'(z)$, the pair $(u(z), v(z))$ for all $z \in (0, \epsilon\ell)$ stays on the invariant curve

$$E_\beta := \{(u, v) : \quad v^2 - u^2 + u^4 = \beta\} \tag{2.10}$$

with some constant $\beta > -\frac{1}{4}$. In particular, it follows from (2.9) that

$$\beta = q^2 - p^2 + p^4 = -p_+^2 + p_+^4. \tag{2.11}$$

Figure 3 shows the (u, v) phase plane and the invariant curve between the points $(p_+, 0)$ and $(p, -q)$. The period function $T_+(p, q)$ defined by

$$T_+(p, q) := \int_p^{p_+} \frac{du}{\sqrt{\beta + u^2 - u^4}} \tag{2.12}$$

gives the z-length of the solution $u(z)$ obtained along the invariant curve E_β between points $(p_+, 0)$ and $(p, -q)$. For the solution $u \in H^2(0, \epsilon\ell)$ in Lemma 2, the relations (2.9) can be written as

$$T_+(p, q) = \epsilon\ell, \quad u(T_+(p, q)) = p, \quad u'(T_+(p, q)) = -q.$$

Compared to the standard terminology, see, e.g., [12], where the period function is introduced for the fundamental period of the periodic function $u(z)$ along the integral curve E_β, the period function $T_+(p, q)$ given by (2.12) corresponds to a part of the integral curve E_β.

The following two lemmas describe properties of the period function $T_+(p, q)$ and the solution $u(z)$ in Lemma 2.
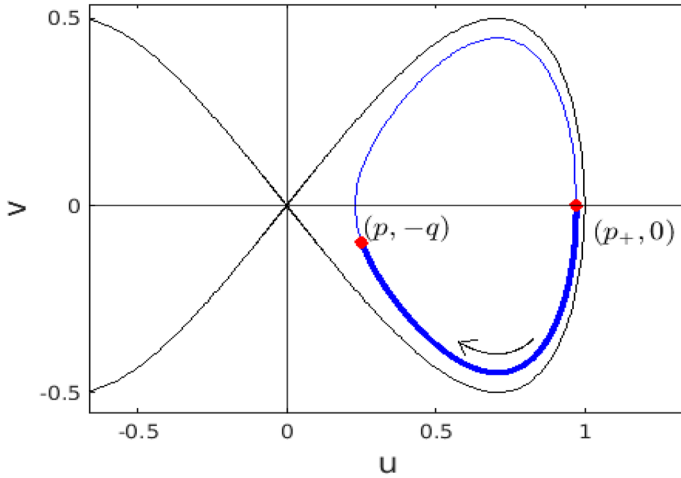
Fig. 3 Phase plane (u, v) for the differential equation $-u'' + u - 2u^3 = 0$ showing the homoclinic loop for $\beta = 0$, the integral curve E_β for $\beta \in (-\frac{1}{4}, 0)$, and the part of the integral curve between points $(p_+, 0)$ and $(p, -q)$

Lemma 3 *There is small $\delta > 0$ such that*

$$\partial_p T_+(p, q) < 0 \quad \text{and} \quad \partial_q T_+(p, q) < 0 \tag{2.13}$$

for every $p \in (0, \delta)$ and $q \in (0, \delta)$.

Proof It follows from the bound (2.8) that

$$T_+(p, q) = -\ln\left(\frac{p + q}{4}\right) + \mathcal{O}\left((p^2 + q^2)(|\ln p| + |\ln q|)\right). \tag{2.14}$$

for small $p > 0$ and $q > 0$. Taking derivatives of (2.14) in p and q justifies the inequalities in (2.13). □

Remark 12 The second property in (2.13) is also proven in Lemma 3.6 of [17] by using more complicated analysis of the integrals in (2.12).

Lemma 4 *Let u be a real, positive, and decreasing solution to the nonlinear equation $-u'' + u - 2u^3 = 0$ on $(0, T_+(p, q))$ satisfying*

$$u(0) = p_+, \quad u'(0) = 0, \quad u(T_+(p, q)) = p, \quad u'(T_+(p, q)) = -q \tag{2.15}$$

with some $p > 0$ and $q > 0$, where p_+ and $T_+(p, q)$ are defined in (2.11) and (2.12). Then, the general solution of the linearized equation $-w''(z) + w(z) - 6u^2(z)w(z) = 0$ is given by

$$w(z) = Au'(z) + Bs(z), \tag{2.16}$$

where A and B are arbitrary parameters and $s(z)$ satisfies $s(0) \neq 0$, $s'(0) = 0$. Moreover, for sufficiently small p and q, u' is negative on $(0, T_+(p, q))$, s vanishes at exactly one point on the interval $(0, T_+(p, q))$ and both functions satisfy

$$\frac{u''(T_+(p, q))}{u'(T_+(p, q))} < 0, \quad \frac{s'(T_+(p, q))}{s(T_+(p, q))} > 0. \tag{2.17}$$

Proof It follows from properties of $u(z)$ in Lemma 2 that $u'(z) < 0$ for $z \in (0, T_+(p, q))$. The first inequality in (2.17) follows from

$$\frac{u''(T_+(p, q))}{u'(T_+(p, q))} = -\frac{p(1 - 2p^2)}{q} < 0, \tag{2.18}$$

for $p \in (0, \frac{1}{\sqrt{2}})$ and $q > 0$.

In order to study the decomposition (2.16), we introduce $s(z) := \partial_q u(z)$ and $r(z) := \partial_p u(z)$, where the parameters p and q are not written in the arguments of $u(z)$, $s(z)$, and $r(z)$. The two functions satisfy the following boundary conditions obtained after differentiating (2.15) with respect to p and q:

$$\begin{cases} s(T_+(p, q)) = q \partial_q T_+, \\ s'(T_+(p, q)) = -1 - p(1 - 2p^2) \partial_q T_+ \end{cases}$$

and

$$\begin{cases} r(T_+(p, q)) = 1 + q \partial_p T_+, \\ r'(T_+(p, q)) = -p(1 - 2p^2) \partial_p T_+. \end{cases}$$

It follows from (2.11) and (2.15) that

$$s(0) = \frac{-q}{p_+(1 - 2p_+^2)}, \quad r(0) = \frac{p(1 - 2p^2)}{p_+(1 - 2p_+^2)}.$$

Since $s'(0) = r'(0) = 0$, uniqueness of solutions of the differential equations implies that the two functions are related by

$$s(z) = -\frac{q}{p(1 - 2p^2)} r(z). \tag{2.19}$$

It follows from the boundary conditions at $z = T_+(p, q)$ and relation (2.19) that

$$\begin{cases} s(T_+(p, q)) = q \partial_q T_+, \\ s'(T_+(p, q)) = q \partial_p T_+, \end{cases} \tag{2.20}$$

so that

$$\frac{s'(T_+(p, q))}{s(T_+(p, q))} = \frac{\partial_p T_+(p, q)}{\partial_q T_+(p, q)} > 0,$$

where positivity follows from (2.13) for sufficiently small p and q.

In order to prove that s vanishes at exactly one point on $(0, T_+(p, q))$, we consider the invariant curve E_β given by (2.10) and the period function $T_+(p, q)$ given by (2.12). Every $z \in (0, T_+(p, q))$ can be represented by $z = T_+(P, Q)$ for some point $(P, Q) \in E_\beta$ with $P \in (p, p_+)$. By Lemma 3.8 in [17], we have $s(z) = 0$ if and only if $\partial_Q T_+(P, Q) = 0$, which also follows from the first equation in system (2.20). Then, by Lemmas 3.6, 3.7, 3.9, 3.10 in [17], for sufficiently small p and q there is exactly one point $(P, Q) \in E_\beta$ with $P \in (p, p_+)$, where $s(z) = s(T_+(P, Q)) = 0$. $\square$

3 Existence of multi-pulse loop-localized states

Here we explain the asymptotic construction of the multi-pulse loop-localized states and give the proof of Theorem 1.

For each boundary vertex $v_j \in \mathcal{V}_B$ with $1 \leq j \leq |B|$, we use the Dirichlet data p_j as the unknown variable and write the flux boundary condition to determine p_j. The main advantage of this method is that the value of p_j can be found independently from the conditions at the other boundary vertices.

Fix j in $1 \leq j \leq |B|$. Assume that the boundary vertex $v_j \in \mathcal{V}_B$ is in contact with K_j pendants, L_j loops, and M_j internal edges from the set $\mathcal{E}_{N,\epsilon}$. We denote the corresponding sets by $\mathcal{E}_{j,\text{pend}}$, $\mathcal{E}_{j,\text{loop}}$, and $\mathcal{E}_{j,\text{int}}$ respectively. Furthermore, we divide $\mathcal{E}_{j,\text{int}}$ into $\mathcal{E}_{j,\text{int}}^-$ and $\mathcal{E}_{j,\text{int}}^+$ depending on whether v_j is the left or right vertex of the internal edge $e \in \mathcal{E}_{j,\text{int}}$, respectively. The large solutions of Lemma 2 are centered at 0 on the pendants and loops but centered at an unknown point $a_e \in (-\epsilon \ell_e, \epsilon \ell_e)$ for $e \in \mathcal{E}_{j,\text{int}}$. Assume *a priori* that for all large ϵ, we have

$$\max_{e \in \mathcal{E}_{j,\text{int}}} |a_e| \leq a_{j,\max}, \tag{3.1}$$

where the constant $a_{j,\max} > 0$ is ϵ-independent.

By Lemma 1, the Neumann data at v_j directed away from $\Gamma_\epsilon \backslash \mathcal{E}_{N,\epsilon}$ is

$$q_j^{(1)} = D_j p_j + \mathcal{O}(\|\mathbf{p}\| e^{-\epsilon \ell_{\min}} + \|\mathbf{p}\|^3), \tag{3.2}$$

where $\mathcal{O}$ denotes the error terms in the bound (2.7).

By Lemma 2, the Neumann data at v_j directed away from $\mathcal{E}_{N,\epsilon}$ is

$$q_j^{(2)} = (K_j + 2L_j + M_j) p_j - 4 \sum_{e \in \mathcal{E}_{j,\text{pend}}} e^{-\epsilon \ell_e} - 8 \sum_{e \in \mathcal{E}_{j,\text{loop}}} e^{-\epsilon \ell_e}$$
$$- 4 \sum_{e \in \mathcal{E}_{j,\text{int}}^-} e^{-\epsilon \ell_e - a_e} - 4 \sum_{e \in \mathcal{E}_{j,\text{int}}^+} e^{-\epsilon \ell_e + a_e} + \mathcal{O}(\epsilon e^{-3\epsilon \ell_{j,\min}}), \tag{3.3}$$

where

$$\ell_{j,\min} := \min\{ \min_{e \in \mathcal{E}_{j,\text{pend}}} \{\ell_e\}, \min_{e \in \mathcal{E}_{j,\text{loop}}} \{\ell_e\}, \min_{e \in \mathcal{E}_{j,\text{int}}} \{\ell_e\}\}$$

and $\mathcal{O}$ denotes the error terms in the bound (2.8). Note that the summation in $q_j^{(2)}$ includes two contributions from the looping edges in $\mathcal{E}_{j,\text{loop}}$ due to the two ends of the looping edge incident to the vertex v_j.

The flux boundary condition in (1.3) gives $q_j^{(1)} + q_j^{(2)} = 0$, which becomes the implicit equation on p_j. Since C^1 property of the error terms is proven in [6] (Remark 10), the implicit equation is immediately solved with

$$
p_j = \frac{4}{Z_j} \left(\sum_{e \in \mathcal{E}_{j,\text{pend}}} e^{-\epsilon \ell_e} + 2 \sum_{e \in \mathcal{E}_{j,\text{loop}}} e^{-\epsilon \ell_e} + \sum_{e \in \mathcal{E}_{j,\text{int}}^-} e^{-\epsilon \ell_e - a_e} + \sum_{e \in \mathcal{E}_{j,\text{int}}^+} e^{-\epsilon \ell_e + a_e} \right)
$$
$$
+ \mathcal{O} \left(\|\mathbf{p}\| e^{-\epsilon \ell_{\min}} + + \|\mathbf{p}\|^3 + \epsilon e^{-3\epsilon \ell_{j,\min}} \right), \tag{3.4}
$$

where $Z_j := D_j + K_j + 2L_j + M_j$ is the total degree of the vertex v_j in Γ_ϵ.

Remark 13 Although the boundary conditions (1.3) are satisfied for all vertices if p_j is defined by (3.4) for $1 \le j \le |B|$, there are two consistency conditions to be verified. One condition arises from the fact that $\|\mathbf{p}\|$ in the error terms in (3.4) include all Dirichlet data $\mathbf{p} = (p_1, p_2, \ldots, p_{|B|})$. Therefore, the error terms in (3.4) must be smaller than the leading-order terms in (3.4) as $\epsilon \to \infty$ for each j. The second condition arises from the fact that the values a_e for $e \in \mathcal{E}_{j,\text{int}}$ must be uniquely defined and be bounded as $\epsilon \to \infty$ according to the *a priori* assumption (3.1).

In order to complete the proof of Theorem 1, it remains to verify the two consistency conditions in Remark 13 from the two technical assumptions, Assumptions 1 and 2.

The first consistency condition is satisfied if

$$
\|\mathbf{p}\| e^{-\epsilon \ell_{\min}} \ll e^{-\epsilon \ell_{j,\min}}, \quad \|\mathbf{p}\|^3 \ll e^{-\epsilon \ell_{j,\min}}, \quad 1 \le j \le |B|,
$$

where $e^{-\epsilon \ell_{j,\min}}$ defines the size of the leading-order terms in (3.4). This leads to the constraints (1.9) and (1.10) in Assumption 1.

The second consistency condition can be formulated in terms of the invariant curve (2.10). The same level β for the large solution of Lemma 2 on a given internal edge must correspond to two segments extending to two different boundary vertices.

Let $e_0 \in \mathcal{E}_{N,\epsilon}$ be an internal edge connecting $v_j \in \mathcal{V}_B$ at the left end and $v_k \in \mathcal{V}_B$ at the right end, so that $e_0 \in \mathcal{E}_{j,\text{int}}^-$ and $e_0 \in \mathcal{E}_{k,\text{int}}^+$ and $j \ne k$. Then, a_{e_0} must be found from the following equation

$$
q_{e_0 \sim v_j}^2 - p_j^2 + p_j^4 = q_{e_0 \sim v_k}^2 - p_k^2 + p_k^4, \tag{3.5}
$$

where $q_{e_0 \sim v_j}$ and $q_{e_0 \sim v_k}$ are given by the expansion

$$
\begin{cases} q_{e_0 \sim v_j} = 4e^{-\epsilon \ell_{e_0} - a_{e_0}} - p_j + \mathcal{O}(\epsilon e^{-3\epsilon \ell_{e_0}}), \\ q_{e_0 \sim v_k} = -4e^{-\epsilon \ell_{e_0} + a_{e_0}} + p_k + \mathcal{O}(\epsilon e^{-3\epsilon \ell_{e_0}}), \end{cases} \tag{3.6}
$$

due to the bounds (2.8).

Let us now assume that the internal edge $e_0 \in \mathcal{E}_{N,\epsilon}$ does not have common boundary vertices with other internal edges in $\mathcal{E}_{N,\epsilon}$ as in Assumption 2. This means that $\mathcal{E}_{j,\text{int}} = \{e_0\}$ and $\mathcal{E}_{k,\text{int}} = \{e_0\}$. Substituting (3.4) and (3.6) into the two sides of equation (3.5) gives the expansions:

$$
\begin{aligned}
q^2_{e_0 \sim v_j} - p^2_j + p^4_j = \frac{16}{Z_j} \Bigg[& (Z_j - 2)e^{-2\epsilon \ell_{e_0} - 2a_{e_0}} \\
& - 2e^{-\epsilon \ell_{e_0} - a_{e_0}} \left(\sum_{e \in \mathcal{E}_{j,\text{pend}}} e^{-\epsilon \ell_e} + 2 \sum_{e \in \mathcal{E}_{j,\text{loop}}} e^{-\epsilon \ell_e} \right) \Bigg] \\
& + \mathcal{O} \Big(\|\mathbf{p}\| e^{-\epsilon \ell_{\min} - \epsilon \ell_0} + + \|\mathbf{p}\|^3 e^{-\epsilon \ell_0} + \epsilon e^{-3\epsilon \ell_{j,\min} - \epsilon \ell_{e_0}} \\
& + e^{-4\epsilon \ell_{j,\min}} + \epsilon e^{-3\epsilon \ell_{e_0} - \epsilon \ell_{j,\min}} + \epsilon e^{-4\epsilon \ell_{e_0}} \Big)
\end{aligned}
$$

and

$$
\begin{aligned}
q^2_{e_0 \sim v_k} - p^2_k + p^4_k = \frac{16}{Z_k} \Bigg[& (Z_k - 2)e^{-2\epsilon \ell_{e_0} + 2a_{e_0}} \\
& - 2e^{-\epsilon \ell_{e_0} + a_{e_0}} \left(\sum_{e \in \mathcal{E}_{k,\text{pend}}} e^{-\epsilon \ell_e} + 2 \sum_{e \in \mathcal{E}_{k,\text{loop}}} e^{-\epsilon \ell_e} \right) \Bigg] \\
& + \mathcal{O} \Big(\|\mathbf{p}\| e^{-\epsilon \ell_{\min} - \epsilon \ell_0} + + \|\mathbf{p}\|^3 e^{-\epsilon \ell_0} + \epsilon e^{-3\epsilon \ell_{k,\min} - \epsilon \ell_{e_0}} \\
& + e^{-4\epsilon \ell_{k,\min}} + \epsilon e^{-3\epsilon \ell_{e_0} - \epsilon \ell_{k,\min}} + \epsilon e^{-4\epsilon \ell_{e_0}} \Big).
\end{aligned}
$$

By Remark 1, we have $Z_j \geq 3$ and $Z_k \geq 3$ for the internal edge e_0. Equating the two sides in (3.5) and dividing by $e^{-2\epsilon \ell_{e_0}}$ gives the unique solution of the implicit equation:

$$
e^{4a_{e_0}} = \frac{(Z_j - 2)Z_k}{(Z_k - 2)Z_j} + E_0, \tag{3.7}
$$

where the error terms in E_0 are given by

$$
\begin{aligned}
E_0 = {} & \frac{2}{Z_k - 2} e^{3a_{e_0} + \epsilon \ell_{e_0}} \left(\sum_{e \in \mathcal{E}_{k,\text{pend}}} e^{-\epsilon \ell_e} + 2 \sum_{e \in \mathcal{E}_{k,\text{loop}}} e^{-\epsilon \ell_e} \right) \\
& - \frac{2Z_k}{Z_j(Z_k - 2)} e^{a_{e_0} + \epsilon \ell_{e_0}} \left(\sum_{e \in \mathcal{E}_{j,\text{pend}}} e^{-\epsilon \ell_e} + 2 \sum_{e \in \mathcal{E}_{j,\text{loop}}} e^{-\epsilon \ell_e} \right) \\
& + \mathcal{O} \Big(\|\mathbf{p}\| e^{\epsilon \ell_{e_0} - \epsilon \ell_{\min}} + + \|\mathbf{p}\|^3 e^{\epsilon \ell_{e_0}} + \epsilon e^{\epsilon \ell_{e_0} - 3\epsilon \ell_{j,\min}} + \epsilon e^{\epsilon \ell_{e_0} - 3\epsilon \ell_{k,\min}} \Big)
\end{aligned}
$$

$$+\mathcal{O}\left(e^{2\epsilon\ell_{e_0}-4\epsilon\ell_{j,\min}} + e^{2\epsilon\ell_{e_0}-4\epsilon\ell_{k,\min}} + \epsilon e^{-\epsilon\ell_{e_0}-\epsilon\ell_{j,\min}} + \epsilon e^{-\epsilon\ell_{e_0}-\epsilon\ell_{k,\min}} + \epsilon e^{-2\epsilon\ell_{e_0}}\right).$$

The error terms beyond the first (leading-order) term in (3.7) are small if

$$\|\mathbf{p}\|e^{-\epsilon\ell_{\min}} \ll e^{-\epsilon\ell_{e_0}},$$
$$\|\mathbf{p}\|^3 \ll e^{-\epsilon\ell_{e_0}},$$
$$\epsilon e^{-3\epsilon\ell_{j,\min}} \ll e^{-\epsilon\ell_{e_0}},$$
$$\epsilon e^{-3\epsilon\ell_{k,\min}} \ll e^{-\epsilon\ell_{e_0}},$$
$$e^{-\epsilon\ell_e} \ll e^{-\epsilon\ell_{e_0}}, \quad \forall e \in \mathcal{E}_{j,\mathrm{pend}} \cup \mathcal{E}_{j,\mathrm{loop}},$$
$$e^{-\epsilon\ell_e} \ll e^{-\epsilon\ell_{e_0}}, \quad \forall e \in \mathcal{E}_{k,\mathrm{pend}} \cup \mathcal{E}_{k,\mathrm{loop}}.$$

The first two conditions coincide with the consistency conditions satisfied by Assumption 1. The other four conditions are satisfied if ℓ_{e_0} is strictly minimal among the half-lengths of the looping edges and the lenghts of the pendant edges as in Assumption 2. This means that

$$\ell_{e_0} = \ell_{j,\min} = \ell_{k,\min} < \ell_e, \quad \forall e \in \mathcal{E}_{j,\mathrm{pend}} \cup \mathcal{E}_{j,\mathrm{loop}} \cup \mathcal{E}_{k,\mathrm{pend}} \cup \mathcal{E}_{k,\mathrm{loop}}.$$

Since the first (leading-order) term in (3.7) is independent of ϵ, the *a priori* assumption (3.1) on the admissible values of a_{e_0} is satisfied by the solution (3.7).

The proof of Theorem 1 is complete. The bound (1.11) follows from the bound (2.24) in Theorem 2.9 in [6].

Remark 14 If two or more internal edges in $\mathcal{E}_N$ are connected to the same vertex, a system of two or more equations (3.5) is set up and the solution for a_{e_0} is no longer available in the simple form (3.7). It is generally hard to obtain the solution for a_{e_0} on each internal edge in the system of nonlinear equations.

4 Morse index for multi-pulse edge-localized states

Here we count the Morse index for multi-pulse edge-localized states and give the proof of Theorem 2.

Let Φ be the positive N-pulse edge-localized state of Theorem 1 such that the set $\mathcal{E}_N$ only contains pendant and looping edges. Let $\mathcal{L} : H^2_{\mathrm{NK}}(\Gamma) \subset L^2(\Gamma) \to L^2(\Gamma)$ be the linearized operator with the differential expression given by (1.8). The number of its negative eigenvalues (the Morse index) is denoted by $n(\mathcal{L})$ and the multiplicity of its zero eigenvalue is denoted by $z(\mathcal{L})$. We will prove that $n(\mathcal{L}) = N$ and $z(\mathcal{L}) = 0$ for large enough ϵ.

Applying the scaling transformation $\Phi(x) = \epsilon U(z)$ with $z = \epsilon x$ and $\epsilon := \sqrt{-\omega}$, we rewrite the spectral problem for $\mathcal{L}$ as a collection of differential equations

$$-w_j''(z) + w_j(z) - 6u_j(z)^2 w_j(z) = \lambda w_j(z), \quad z \in e_{j,\epsilon}, \tag{4.1}$$

subject to the boundary conditions (1.3) at vertices $v \in \mathcal{V}$. Here $W = (w_1, w_2, \ldots, w_{|\mathcal{E}|})$ is a rescaled eigenvector in $H^2_{NK}(\Gamma_\epsilon)$ and λ is a rescaled eigenvalue of the linearized operator $\mathcal{L}$. Abusing notations, we still refer to the linearized operator in the rescaled variables as to $\mathcal{L}$.

4.1 Idea of the proof

Recall that $\mathcal{V}_B$ is the set of boundary vertices separating $\mathcal{E}_{N,\epsilon}$ and $\Gamma_\epsilon \backslash \mathcal{E}_{N,\epsilon}$. Then for every $\boldsymbol{\alpha} = (\alpha_1, \alpha_2, \cdots, \alpha_{|B|})$, let the space $H^2_{\boldsymbol{\alpha}}(\Gamma_\epsilon)$ be defined by the modified boundary conditions:

$$\begin{cases} W \text{ is continuous on } \Gamma_\epsilon, \\ \sum_{e \sim v} \partial W(v) = 0 \text{ for every vertex } v \in \mathcal{V} \backslash \mathcal{V}_B, \\ \sum_{e \sim v_j} \partial W(v_j) = \alpha_j W(v_j) \text{ for every vertex } v_j \in \mathcal{V}_B, \end{cases} \tag{4.2}$$

where the derivatives ∂ are directed away from the vertex.

We use $\boldsymbol{\alpha} = 0$ to denote $\boldsymbol{\alpha} = (0, 0, \ldots, 0)$ and $\boldsymbol{\alpha} = \infty$ to denote $\boldsymbol{\alpha} = (+\infty, +\infty, \ldots, +\infty)$. Then, we have $H^2_{NK}(\Gamma_\epsilon) \equiv H^2_{\boldsymbol{\alpha}=0}(\Gamma_\epsilon)$ and $H^2_D(\Gamma_\epsilon) \equiv H^2_{\boldsymbol{\alpha}=\infty}(\Gamma_\epsilon)$, where $H^2_D(\Gamma_\epsilon)$ stands for the domain with the Dirichlet conditions at the boundary vertices:

$$\begin{cases} W \text{ is continuous on } \Gamma_\epsilon, \\ \sum_{e \sim v} \partial W(v) = 0 \text{ for every vertex } v \in \mathcal{V} \backslash \mathcal{V}_B, \\ W(v_j) = 0 \text{ for every vertex } v_j \in \mathcal{V}_B. \end{cases} \tag{4.3}$$

We also introduce the linearized operator $\mathcal{L}_{\boldsymbol{\alpha}}$, such that the spectral problem $\mathcal{L}_{\boldsymbol{\alpha}} W = \lambda W$ is still represented by the differential equations (4.1), but the domain of $\mathcal{L}_{\boldsymbol{\alpha}}$ is $H^2_{\boldsymbol{\alpha}}(\Gamma_\epsilon) \subset L^2(\Gamma_\epsilon)$.

The proof of Theorem 2 relies on the continuity argument from $\boldsymbol{\alpha} = \infty$ to $\boldsymbol{\alpha} = 0$ given by the following proposition.

Proposition 1 *Assume that $\mathcal{L}_{\boldsymbol{\alpha}} W = 0$ admits no solutions $W \in H^2_{\boldsymbol{\alpha}}(\Gamma_\epsilon)$ for every $\boldsymbol{\alpha} \in [0, \infty)^{|B|}$. Then, we have $n(\mathcal{L}_{\boldsymbol{\alpha}=0}) = n(\mathcal{L}_{\boldsymbol{\alpha}=\infty})$ and $z(\mathcal{L}_{\boldsymbol{\alpha}=0}) = 0$.*

Proof The proof relies on the standard perturbation theory of linear operators given in Chapter 7 of [18]. Since $\mathcal{L}_{\boldsymbol{\alpha}}$ is a holomorphic family of self-adjoint operators, each isolated eigenvalue of $\mathcal{L}_{\boldsymbol{\alpha}}$ depends continuously on α. Therefore, if no eigenvalues of $\mathcal{L}_{\boldsymbol{\alpha}}$ cross zero when $\boldsymbol{\alpha}$ traverses from $\boldsymbol{\alpha} = \infty$ to $\boldsymbol{\alpha} = 0$, then the number of negative eigenvalues remains the same. $\qquad\square$

By using Proposition 1, Theorem 2 holds if we can verify the following claims for large ϵ:

Claim 1: $n(\mathcal{L}_{\boldsymbol{\alpha}=\infty}) = N$;

Claim 2: $\mathcal{L}_{\boldsymbol{\alpha}} W = 0$ admits no solutions $W \in H^2_{\boldsymbol{\alpha}}(\Gamma_\epsilon)$ with $\alpha \in [0, \infty)^{|B|}$.

Below we give proofs of these claims.

4.2 Proof of Claim 1

The proof is based on the Sturm's Comparison theorem (see Sect. 5.5 in [27]). For simplicity, we assume that $\mathcal{E}_N$ contains only looping edges. Due to the symmetry of solutions in the looping edges with respect to the middle point, the proof extends to the pendant edges with minor modifications.

The spectral problem for the operator $\mathcal{L}_{\boldsymbol{\alpha}=\infty}$ can be expressed by the second-order differential equations (4.1) equipped with the Dirichlet conditions at the boundary vertices given by (4.3). The spectral problem for $\mathcal{L}_{\boldsymbol{\alpha}=\infty}$ is given by N uncoupled problems on the N edges in $\mathcal{E}_{N,\epsilon}$ and another uncoupled problem in $\Gamma_\epsilon \backslash \mathcal{E}_{N,\epsilon}$. On each edge $e_{j,\epsilon} \in \mathcal{E}_{N,\epsilon}$, we have

$$\begin{cases} -w_j''(z) + w_j(z) - 6u_j(z)^2 w_j(z) = \lambda w_j(z), & z \in (-\epsilon\ell_j, \epsilon\ell_j), \\ w_j(-\epsilon\ell_j) = w_j(\epsilon\ell_j) = 0, \end{cases} \tag{4.4}$$

where $u_j(z)$ satisfies the condition (2.5). Since ϵ is large, $p := u(\epsilon\ell_j)$ and $q := -u'(\epsilon\ell_j)$ are small and positive by Lemma 2. For $\lambda = 0$, the homogeneous equation (4.4) is solved by the superposition formula (2.16) in Lemma 4, where the even solution $s(z)$ has exactly one nodal point on $(0, \epsilon\ell_j)$ and the odd solution $u'(z)$ has no nodal points on $(0, \epsilon\ell_j)$. By Sturm's Comparison theorem, the spectral problem (4.4) admits exactly one simple negative eigenvalue. Since eigenvalues of all N spectral problems (4.4) also appear in the spectrum of the operator $\mathcal{L}_{\boldsymbol{\alpha}=\infty}$, we have $n(\mathcal{L}_{\boldsymbol{\alpha}=\infty}) \geq N$.

Remark 15 If $e_{j,\epsilon} \in \mathcal{E}_{N,\epsilon}$ is a pendant edge, the Neumann condition at one end implies that the spectral problem (4.4) is solved in the space of even functions, where it still admits exactly one simple negative eigenvalue and no zero eigenvalue.

Next, we show that the uncoupled problem in $\Gamma_\epsilon \backslash \mathcal{E}_{N,\epsilon}$ given by

$$-W'' + W - 6U^2 W = \lambda W, \quad z \in \Gamma_\epsilon \backslash \mathcal{E}_{N,\epsilon}, \tag{4.5}$$

subject to the boundary conditions (4.3) has a strictly positive spectrum. Since U on $\Gamma_\epsilon \backslash \mathcal{E}_{N,\epsilon}$ satisfies the bound (2.6) with small $\mathbf{p}$ given by (3.4), we obtain from (4.5) after multiplication by W and integration over $\Gamma_\epsilon \backslash \mathcal{E}_{N,\epsilon}$ with the boundary conditions (4.3):

$$\lambda \|W\|_{L^2(\Gamma_\epsilon \backslash \mathcal{E}_{N,\epsilon})}^2 = \|W\|_{L^2(\Gamma_\epsilon \backslash \mathcal{E}_{N,\epsilon})}^2 - 6\|UW\|_{L^2(\Gamma_\epsilon \backslash \mathcal{E}_{N,\epsilon})}^2 + \|W'\|_{L^2(\Gamma_\epsilon \backslash \mathcal{E}_{N,\epsilon})}^2$$
$$\geq C\|W\|_{L^2(\Gamma_\epsilon \backslash \mathcal{E}_{N,\epsilon})}^2,$$

for some $C > 0$. Hence, $\lambda \geq C > 0$ for every solution $W \in H_{\mathrm{D}}^2((\Gamma_\epsilon \backslash \mathcal{E}_{N,\epsilon}))$, and the spectral problem (4.5) does not contribute into the nonpositive part of the spectrum of the operator $\mathcal{L}_{\boldsymbol{\alpha}=\infty}$. This completes the proof of $n(\mathcal{L}_{\boldsymbol{\alpha}=\infty}) = N$.

4.3 Proof of Claim 2

Let W be a solution of $\mathcal{L}_\alpha W = 0$ in $H^2(\Gamma_\epsilon)$ with large enough ϵ. For every looping edge $e_{j,\epsilon} \in \mathcal{E}_{N,\epsilon}$ associated with the segment $[-\epsilon\ell_j, \epsilon\ell_j]$, the restriction of W to the edge $e_{j,\epsilon}$ denoted by w_j solves the second-order differential equation

$$- w_j''(z) + w_j(z) - 6u_j(z)^2 w_j(z) = 0, \quad z \in (-\epsilon\ell_j, \epsilon\ell_j). \qquad (4.6)$$

where $u_j(z)$ satisfies the condition (2.5). The following lemma computes the contributions of the solution of the differential equation (4.6) to the last boundary condition in (4.2).

Lemma 5 *If $e_{j,\epsilon} \in \mathcal{E}_{N,\epsilon}$ is a looping edge with ϵ large enough, then either $w_j \equiv 0$ on the entire edge or*

$$\alpha_\pm(e_{j,\epsilon}) := \mp\frac{w_j'(\pm\epsilon\ell_j)}{w_j(\pm\epsilon\ell_j)} < 0. \qquad (4.7)$$

Proof By Lemma 4, the general solution is given by (2.16) rewritten again as

$$w_j(z) = Au_j'(z) + Bs_j(z) \qquad (4.8)$$

for some parameters A and B. Since $u_j'(z)$ is odd, $s_j(z)$ is even, and $u_j'(\pm\epsilon\ell_j) \neq 0$, the continuity condition $w_j(-\epsilon\ell_j) = w_j(\epsilon\ell_j)$ necessarily implies $A = 0$.

If $B = 0$, then $w_j \equiv 0$ on the entire edge. If $B \neq 0$, then $w_j(\pm\epsilon\ell_j) \neq 0$ and $\alpha_\pm(e_{j,\epsilon})$ in (4.7) is defined by $s_j(\pm\epsilon\ell_j)$ and $s_j'(\pm\epsilon\ell_j)$. It follows from the second inequality in (2.17) and the symmetry of $s_j(z)$ that $\alpha_\pm(e_{j,\epsilon}) < 0$. □

Remark 16 If $e_{j,\epsilon} \in \mathcal{E}_{N,\epsilon}$ is a pendant edge, the Neumann condition at one end still implies that $A = 0$ in the general solution (4.8), after which the proof of Lemma 5 holds and gives $\alpha_+(e_{j,\epsilon}) < 0$.

We denote the value of W at each boundary point $v_j \in \mathcal{V}_B$ as $\mathfrak{p}_j := W(v_j)$. Then on the subgraph $\Gamma_\epsilon \backslash \mathcal{E}_{N,\epsilon}$, W solves the homogeneous equation

$$- W'' + W - 6U^2 W = 0, \quad z \in \Gamma_\epsilon \backslash \mathcal{E}_{N,\epsilon}, \qquad (4.9)$$

subject to the nonhomogeneous Dirichlet boundary conditions:

$$\begin{cases} W \text{ is continuous on } \Gamma_\epsilon \backslash \mathcal{E}_{N,\epsilon}, \\ \sum_{e \sim v} \partial W(v) = 0 \text{ for every vertex } v \in \mathcal{V} \backslash \mathcal{V}_B, \\ W(v_j) = \mathfrak{p}_j \text{ for every vertex } v_j \in \mathcal{V}_B. \end{cases} \qquad (4.10)$$

The following lemma computes the contributions of the solution of the boundary-value problem (4.9)–(4.10) to the last boundary condition in (4.2).

Lemma 6 *There are $C_0 > 0$ and $\epsilon_0 > 0$ such that for every $\mathfrak{p} = (\mathfrak{p}_1, \mathfrak{p}_2, \ldots, \mathfrak{p}_{|B|})$ and every $\epsilon > \epsilon_0$, the unique solution $W \in H^2(\Gamma_\epsilon \backslash \mathcal{E}_{N,\epsilon})$ of the boundary-value problem (4.9)–(4.10) satisfies*

$$\|W\|_{H^2(\Gamma_\epsilon \backslash \mathcal{E}_{N,\epsilon})} \leq C_0 \|\mathfrak{p}\| \tag{4.11}$$

and

$$|\mathfrak{q}_j - D_j \mathfrak{p}_j| \leq C_0 \|\mathfrak{p}\| e^{-\epsilon \ell_{\min}}, \tag{4.12}$$

where $\mathfrak{q}_j$ is the Neumann data directed away from $\Gamma_\epsilon \backslash \mathcal{E}_{N,\epsilon}$, D_j is the degree of the j-th boundary vertex $v_j \in \mathcal{V}_B$ in $\Gamma_\epsilon \backslash \mathcal{E}_{N,\epsilon}$, and $\ell_{\min}$ is the length of the shortest edge in $\Gamma \backslash \mathcal{E}_N$.

Proof Since $\|U\|_{L^\infty(\Gamma_\epsilon \backslash \mathcal{E}_{N,\epsilon})}$ is small for large enough ϵ by the bound (2.6) with $\mathbf{p}$ given by (3.4), the boundary-value problem (4.9)–(4.10) can be analyzed with Theorem 2.1 and Lemma 2.3 in [6] for $g = 0$. The bounds (4.11) and (4.12) follow from the bounds (2.3) and (2.4) in [6] due to the smallness of $\|U\|_{L^\infty(\Gamma_\epsilon \backslash \mathcal{E}_{N,\epsilon})}$. □

Remark 17 The Neumann data $\mathfrak{q}_j$ in (4.12) is directed in the opposite direction compared to $\partial W(v_j)$ in (4.2). In other words,

$$\sum_{e \sim v_j, e \in \Gamma_\epsilon \backslash \mathcal{E}_{N,\epsilon}} \partial W(v_j) = -\mathfrak{q}_j = -D_j \mathfrak{p}_j + \mathcal{O}(\|\mathfrak{p}\| e^{\epsilon \ell_{\min}}). \tag{4.13}$$

We are now ready to show that no solutions $W \in H^2(\Gamma_\epsilon)$ of $\mathcal{L}_{\boldsymbol{\alpha}} W = 0$ satisfy the last boundary condition in (4.2) with α_j being nonnegative.

First, we consider the case when $\mathfrak{p}_j = 0$ for all $v_j \in \mathcal{V}_B$. Then, the right hand side of the last boundary conditions in (4.2) vanishes and W satisfies the Neumann-Kirchhoff (NK) boundary conditions. Moreover, by Lemma 5, the $\mathcal{E}_{N,\epsilon}$-components of the solution W are entirely zero, and make no contribution into the last condition in (4.2). In what follows, the restriction of W to $\Gamma_\epsilon \backslash \mathcal{E}_{N,\epsilon}$ solves the second-order differential equation (4.9) subject to the Dirichlet conditions at the boundary vertices. By Lemma 6 due to the bound (4.11), the only solution on $\Gamma_\epsilon \backslash \mathcal{E}_{N,\epsilon}$ is zero, hence $W \equiv 0$ on Γ_ϵ.

Therefore, there exists at least one boundary vertex $v_j \in \mathcal{V}_B$ such that the corresponding $\mathfrak{p}_j \neq 0$. Up to multiplication by a constant, we may assume that $\mathfrak{p}_j = 1$. Using Lemmas 5 and 6 and the expansion (4.13), the last condition in (4.2) for large enough ϵ becomes

$$\alpha_j = \sum_{e \in \mathcal{E}_{j,\epsilon}} \alpha_-(e) + \sum_{e \in \mathcal{E}_{j,\epsilon}} \alpha_+(e) - \mathfrak{q}_j < 0, \tag{4.14}$$

where $\mathcal{E}_{j,\epsilon} \subset \mathcal{E}_{N,\epsilon}$ is the set of edges in $\mathcal{E}_{N,\epsilon}$ adjacent to the vertex $v_j \in \mathcal{V}_B$. This contradicts to the assumption that $\alpha_j \in [0, \infty)$. Hence no $W \in H_{\boldsymbol{\alpha}}^2(\Gamma_\epsilon)$ exists such that $\mathcal{L}_{\boldsymbol{\alpha}} W = 0$ for $\alpha \in [0, \infty)^{|B|}$.
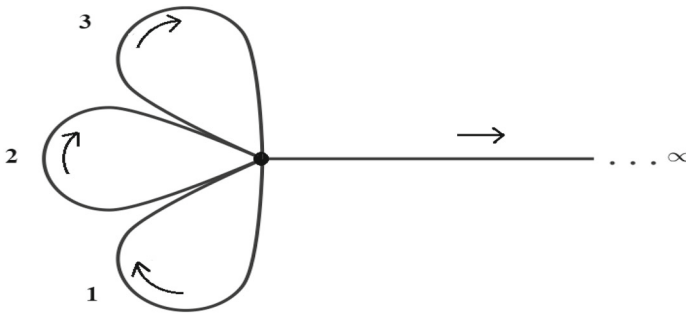
Fig. 4 A flower graph with three loops as in Example 1. Each loop j with $j = 1, 2, 3$ is parametrized by a segment $[-\ell_j, \ell_j]$ of length $2\ell_j$, and the unbounded edge is parametrized by a half-line $[0, \infty)$. The direction of the axis associated with each of the segments is specified by the arrows
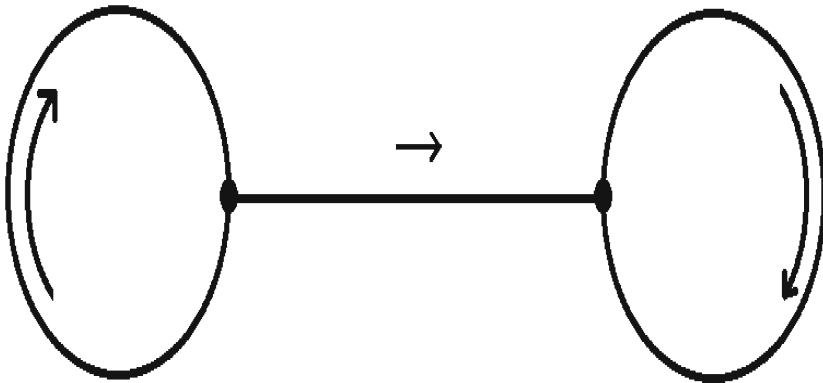

Fig. 5 A dumbbell graph as in Example 2. The left loop is parametrized by a segment $[-\ell_-, \ell_-]$ of length $2\ell_-$, and the right loop is parametrized by a segment $[-\ell_+, \ell_+]$ of length $2\ell_+$. The internal edge is parametrized by a segment $[-\ell_0, \ell_0]$ of length $2\ell_0$. The direction of the axis associated with each of the segments is specified by the arrows

5 Examples

We end this paper with three examples of quantum graphs, where the assumptions of Theorems 1 and 2 can be checked. We also discuss limitations of results of Theorems 1 and 2 to cover all edge-localized states on these graphs.

Example 1 Consider a flower graph consisting of L loops of the lengths $\{2\ell_j\}_{j=1}^L$ and one half-line connected at a single common vertex, see Fig. 4 for $L = 3$. Assumption 1 is satisfied because $|B| = 1$ (Remark 2). Assumption 2 is satisfied because no internal edges exist. Theorem 1 states existence of the N-pulse edge-localized states for every $1 \leq N \leq L$ and Theorem 2 states that Morse index of this N-pulse state is N. This coincides with the main results of [17] (Theorems 1, 2, and 3) in the limit $\omega \to -\infty$ obtained with long analysis of the period function in the case of loops of the same normalized length.

Example 2 Consider a dumbbell graph consisting of two loops of lengths $2\ell_-$ and $2\ell_+$ connected by an internal edge of length $2\ell_0$ at two vertices, see Fig. 5. Assume that $\ell_- \leq \ell_+$ for convenience. The numerical approximations were performed by using the Quantum Graph Package [13] for $\ell_- = \ell_+ = \pi$, $\ell_0 = 2 < \ell_-$, and fixed $\omega = -4$. Several edge-localized states can be constructed by using Theorem 1 as follows.

- By Theorem 1, assumptions of which are trivially satisfied if $N = 1$, the 1-pulse state can be placed at any of the three edges in the limit $\omega \to -\infty$ in agreement with the main results of [4] and [6]. By Theorem 2, Morse index of the 1-pulse state placed at the loop is 1. Morse index for the 1-pulse state placed at the internal edge is not defined by Theorem 2. By the variational theory in [4], the Morse index of this 1-pulse state is also 1. It was also proven explicitly in Lemma 4.10 in [21] for the symmetric dumbbell graph with $\ell_- = \ell_+$ that the Morse index of this 1-pulse state is 1. Figure 6a, b show the 1-pulse states and we have confirmed that the Morse index of each state is 1.

- By Theorem 1, the 2-pulse state can be placed at the two loops if $\ell_+ < 2\ell_0 + \ell_-$ and $\ell_+ < 3\ell_-$ from the conditions (1.9) and (1.10) respectively. The constraints are satisfied if $\ell_- = \ell_+$. By Theorem 2, the Morse index of this 2-pulse state is 2. Figure 6c shows this 2-pulse state and we have confirmed that the Morse index is 2.

- By Theorem 1, the 2-pulse state can also be placed at one loop and the internal edge if $\ell_0 < \ell_- \leq \ell_+$ due to Assumption 2. The conditions (1.9) and (1.10) of Assumption 1 are satisfied if $\ell_0 < \ell_- \leq \ell_+$. The Morse index of this 2-pulse state is not defined by Theorem 2. Figure 6d shows this 2-pulse state. Numerical computations show that the Morse index of this state is $3 > N = 2$.

- By Theorem 1, the 3-pulse state can be placed at all three edges if $\ell_0 < \ell_- \leq \ell_+$. The Morse index of this 3-pulse state is not defined by Theorem 2. Figure 6e shows this 3-pulse state. Numerical computations show that the Morse index of this state is $5 > N = 3$.

Example 3 Consider a graph Γ which is given in Fig. 7. It formally consists of three edges, where $e_1 = [0, \ell_1]$ and $e_3 = [0, \ell_3]$ are pendant edges and $e_2 = [-\ell_2, \ell_2]$ is the internal edge. However, v_2 and v_3 have are dummy vertices of degree 2, hence the same graph is mapped into a single interval $[-\ell_1 - \ell_2, \ell_2 + \ell_3]$ subject to Neumann boundary conditions at the end points. Assume that $\ell_1 \leq \ell_3$ for convenience.

All possible solutions of the Neumann boundary-value problem for the stationary equation $-u'' + u - 2u^3 = 0$ are given by the integral curves shown on Fig. 8. Due to the Neumann boundary conditions, the positive solution starts and ends at one of the two points $(p_-, 0)$ and $(p_+, 0)$ shown in red. Besides two simplest states localized at one of the two pendant edges from a half-loop on Fig. 8, we can construct three additional edge-localized states as follows.

- Let us take a single loop on the integral curve of Fig. 8 with the boundary conditions

$$u(-\epsilon(\ell_1 + \ell_2)) = u(\epsilon(\ell_2 + \ell_3)) = p_-.$$

Due to the spatial symmetry, the 1-pulse state concentrates at the middle point $z = \frac{1}{2}\epsilon(\ell_3 - \ell_1)$. Since $\ell_1 \leq \ell_3$ implies $\ell_1 < 2\ell_2 + \ell_3$, the middle point belongs
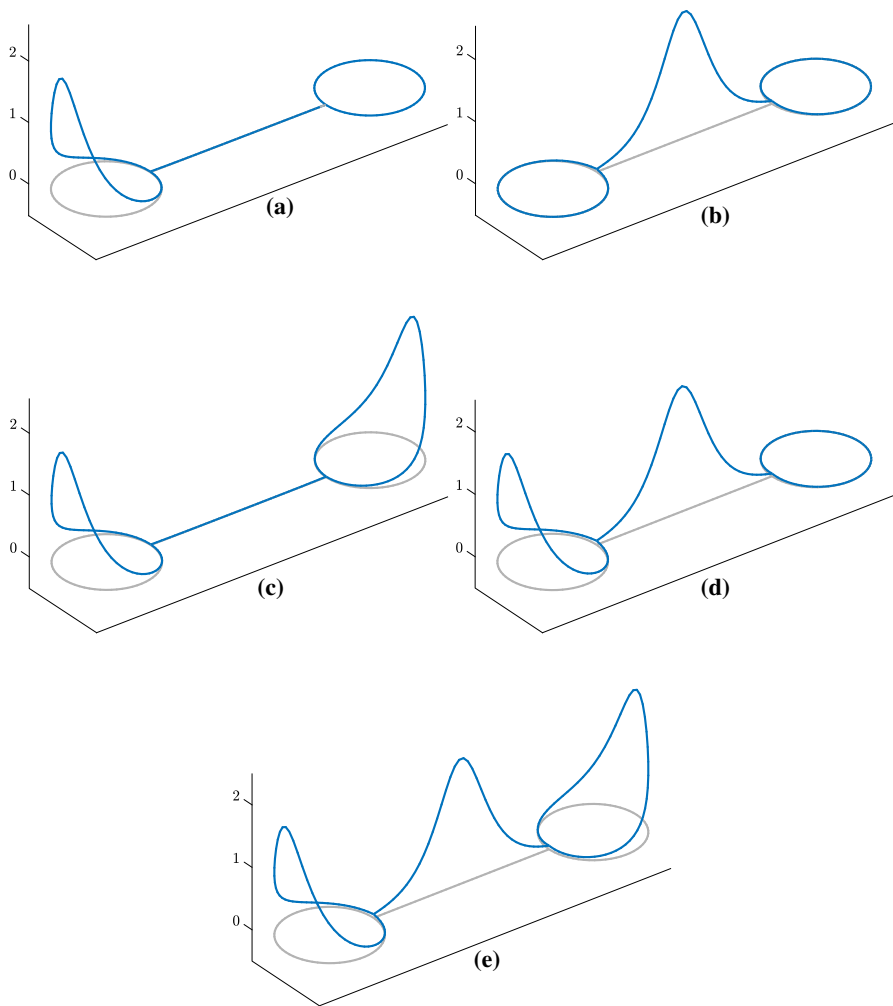
Fig. 6 Five edge-localized states on the dumbbell graph with $\ell_- = \ell_+ = \pi$, $\ell_0 = 2$, and $\omega = -4$
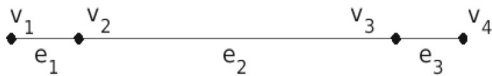

Fig. 7 A segment graph Γ in Example 3

to e_2, hence the edge-localized state in the limit of large ϵ (when $p_- \rightarrow 0$) corresponds to the choice $\mathcal{E}_1 := \{e_2\}$ for the graph Γ on Fig. 7. This 1-pulse state is illustrated on the left panel of Fig. 9. The right panel shows the derivative $u'(z)$ which satisfies the homogeneous equation $-w''(z) + w(z) - 6u(z)^2 w(z) = 0$ and Dirichlet conditions at the end points of the interval $[-\epsilon(\ell_1 + \ell_2), \epsilon(\ell_2 + \ell_3)]$. Using the Courant's nodal theorem (see Sect. 5.5 in [27]), since $u'(z)$ has two nodal domains on the interval, the zero eigenvalue is the second eigenvalue of the Dirichlet boundary-value problem (denoted as λ_j^D) interlacing with the eigenvalues
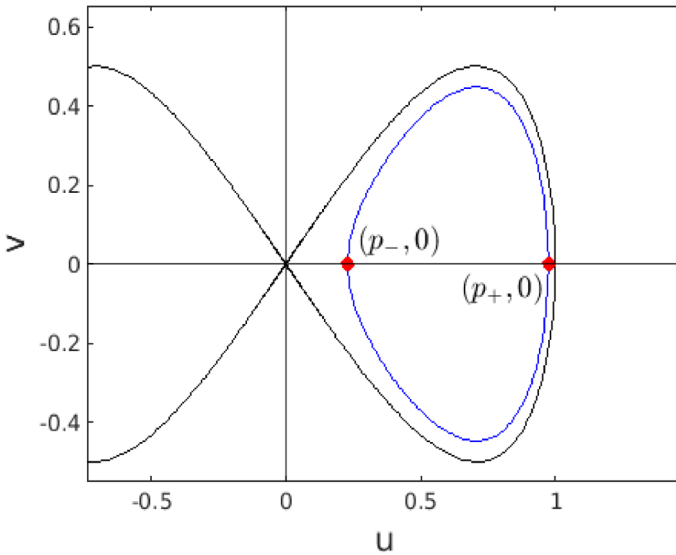
Fig. 8 Phase plane (u, v) of the differential equation $-u'' + u - 2u^3 = 0$ showing the homoclinic loop for $\beta = 0$ and the integral curve E_β for $\beta \in (-\frac{1}{4}, 0)$

of the Neumann boundary-value problem (denoted as λ_j^N) as follows:

$$\lambda_1^N < \lambda_1^D \leq \lambda_2^N < \lambda_2^D = 0 \leq \lambda_3^N < \lambda_3^D \leq \lambda_4^N < \ldots \tag{5.1}$$

Here the inequality between λ_2^N and λ_2^D is strict because the even potential $-6u(z)^2$ of the Schrödinger operator $\partial_z^2 + 1 - 6u(z)^2$ is extended periodically on $\mathbb{R}$ and it is a well-known fact that the anti-periodic eigenfunctions for λ_1^D and λ_2^N can not exist at the same eigenvalues as the periodic eigenfunctions for λ_2^D and λ_3^N. Similarly, the inequality between λ_3^N and λ_3^D is strict. It follows from (5.1) that the Morse index of the 1-pulse state is $n(\mathcal{L}) = 2$. This is a counter-example to conclusion of Theorem 2 with $N = 1$ which is the reason why the internal edges are excluded from the set $\mathcal{E}_N$ in Theorem 2.

- Let us take a single loop on the integral curve of Fig. 8 with the boundary conditions

$$u(-\epsilon(\ell_1 + \ell_2)) = u(\epsilon(\ell_2 + \ell_3)) = p_+.$$

In the limit of large ϵ (when $p_+ \to 1$), this 2-pulse state corresponds to the choice $\mathcal{E}_2 := \{e_1, e_3\}$ for the graph Γ on Fig. 7. Assumption 1 is satisfied if $\ell_+ < 2\ell_0 + \ell_-$ and $\ell_+ < 3\ell_-$. The 2-pulse state exists for sufficiently large ϵ by Theorem 1. This solution is illustrated on the left panel of Fig. 10. The right panel shows the derivative $u'(z)$ with two nodal domains, so that the ordering (5.1) suggests that $n(\mathcal{L}) = 2$. This agrees with the count of Theorem 2 with $N = 2$ since the internal edge e_2 is not in the set $\mathcal{E}_N$ and the dummy vertices v_2 and v_3 are not obstruction to the construction of edge-localized states on the pendant edges.
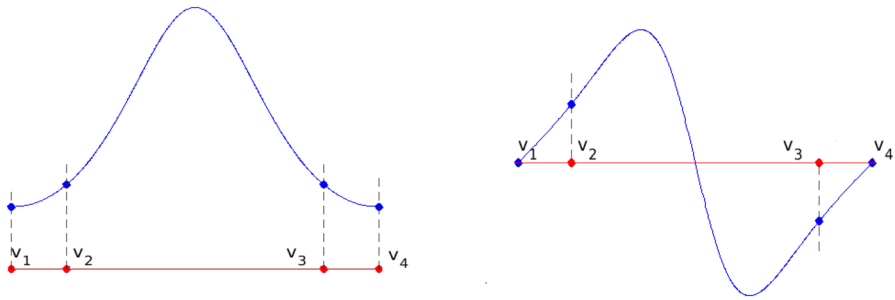
Fig. 9 Left: the 1-pulse state on the internal edge e_2. Right: its derivative satisfying Dirichlet conditions on the interval
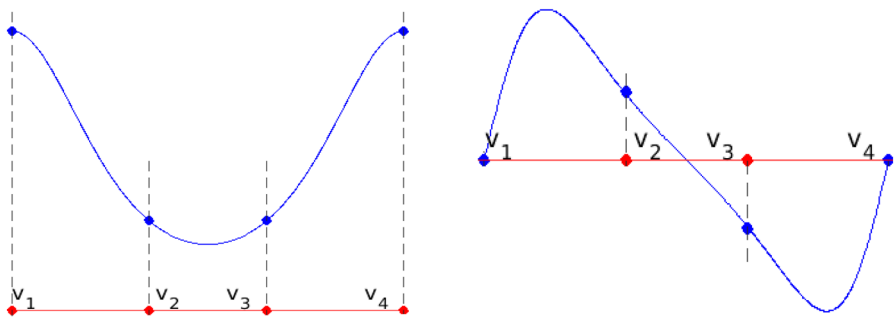

Fig. 10 Left: the 2-pulse state on the two pendants e_1 and e_3. Right: its derivative satisfying Dirichlet conditions on the interval
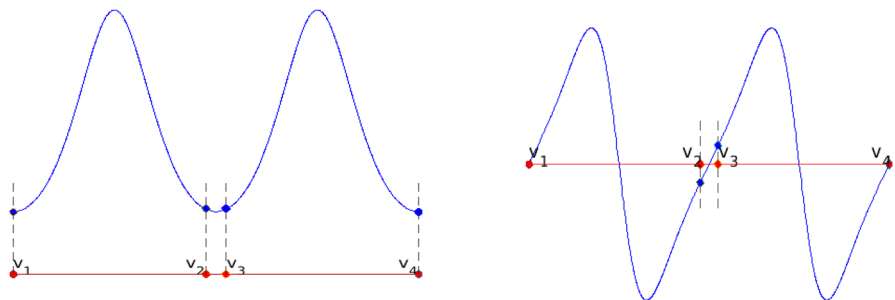

Fig. 11 Left: the 2-pulse state centered in the middle of the two pendants e_1 and e_3. Right: its derivative satisfying Dirichlet conditions on the interval

- Let us take two loops on the integral curve of Fig. 8 with the boundary conditions

$$u(-\epsilon(\ell_1 + \ell_2)) = u(\epsilon(\ell_2 + \ell_3)) = p_-,$$

as shown on Fig. 11. Although $p_- \to 0$ as $\epsilon \to 0$, this 2-pulse state does not correspond to the choice $\mathcal{E}_2 := \{e_1, e_3\}$ in Theorem 1 because the edge-localized states at the pendants must be centered at the ends under the Neumann conditions. Consequently, the derivative $u'(z)$ also shown on Fig. 11 has four nodal domains

suggesting by the Courant's nodal theorem that $n(\mathcal{L}) = 4$ which would contradict Theorem 2 with $N = 2$. However, as we explained, the main results are not applicable to the 2-soliton state which is not localized at the ends of the pendants.

6 Conclusion

We have proven existence of the multi-pulse edge-localized positive states on a general quantum graph in the limit of large mass. The existence results are obtained from nonlinear equations representing the flux boundary condition at the boundary vertices separating N edges where solitons reside from the rest of the graph. Nonlinear equations are solved independently of each other under certain sufficient conditions on the edge lengths of the N edges. We have also computed the Morse index of the multi-pulse states residing on the looping and internal edges.

The sufficient conditions in the main theorems are definitely not sharp conditions on the existence of multi-pulse edge-localized states. The states may exist when these conditions are violated, but the nonlinear equations would have to be solved all together with different analytical methods. Similarly, one can consider existence of non-positive edge-localized states, for which solvability of the nonlinear equation may be delicate even in the limit of large mass.

Our consideration excludes multi-pulse states which are localized at the internal vertices of the quantum graph or in the middle of the pendant edges. Studies of the nonlinear equations from the flux boundary conditions in these situations are open for the future work.

Similarly, Morse index was computed when multi-pulse solutions were not localized at the internal edges of the quantum graph. It is possible that some sharp inequalities instead of equalities can be obtained in a more general setting of internal edges. This work is also left for future studies.

Data availability statement The datasets analysed during the current study are available from the corresponding author on request.

Conflict of interest The authors have no conflict of interests.

References

1. Adami, R., Serra, E., Tilli, P.: NLS ground states on graphs. Calc. Var. **54**, 743–761 (2015)
2. Adami, R., Serra, E., Tilli, P.: Threshold phenomena and existence results for NLS ground states on graphs. J. Funct. Anal. **271**, 201–223 (2016)
3. Adami, R., Serra, E., Tilli, P.: Negative energy ground states for the L^2-critical NLSE on metric graphs. Commun. Math. Phys. **352**, 387–406 (2017)

4. Adami, R., Serra, E., Tilli, P.: Multiple positive bound states for the subcritical NLS equation on metric graphs. Calc. Var. **58**, 5 (2019)
5. Berkolaiko, G., Kuchment, P.: Introduction to Quantum Graphs (Mathematical Surveys and Monographs, vol 186. American Mathematical Society, Providence, RI (2013)
6. Berkolaiko, G., Marzuola, J., Pelinovsky, D.E.: Edge-localized states on quantum graphs in the limit of large mass. Ann. de l'Inst. Henri Poincaré C Anal. Non linéaire **38**, 1295–1335 (2021)
7. Berkolaiko, G., Kennedy, J.B., Kurasov, P., Mugnolo, D.: Surgery principles for the spectral analysis of quantum graphs. Trans. AMS **372**, 5153–5197 (2019)
8. Cacciapuoti, C., Finco, D., Noja, D.: Topology induced bifurcations for the NLS on the tadpole graph. Phys. Rev. E **91**, 013206 (2015)
9. Dovetta, S., Serra, E., Tilli, P.: Uniqueness and non-uniqueness of prescribed mass NLS ground states on metric graphs, Adv. Math. **374** (2020), 107352 (41 pages)
10. Dovetta, S., Ghimenti, M., Micheletti, A.M., Pistoia, A.: Peaked and low action solutions of NLS equations on graphs with terminal edges. SIAM J. Math. Anal. **52**, 2874–2894 (2020)
11. Exner, P., Kovarik, H.: Quantum Waveguides. Theoretical and Mathematical Physics. Springer, Cham (2015)
12. Garijo, A., Villadelprat, J.: Algebraic and analytical tools for the study of the period function. J. Differ. Eqs. **257**, 2464–2484 (2014)
13. Goodman, R.H., Conte, G., Marzuola, J.L.: Quantum Graphs Package, version 0.96 (2021), https://doi.org/10.5281/zenodo.4898112
14. Goodman, R.H.: NLS bifurcations on the bowtie combinatorial graph and the dumbbell metric graph. Discrete Contin. Dyn. Syst. **39**(4), 2203–2232 (2019)
15. Grillakis, M.: Linearized instability for nonlinear Schrödinger and Klein–Gordon equations. Commun. Pure Appl. Math. **41**, 747–774 (1988)
16. Grillakis, M., Shatah, J., Strauss, W.: Stability theory of solitary waves in the presence of symmetry I. J. Funct. Anal. **74**, 160–197 (1987)
17. Kairzhan, A., Marangell, R., Pelinovsky, D.E., Xiao, K.: Standing waves on a flower graph. J. Differ. Eqs. **271**, 719–763 (2021)
18. Kato, T.: Perturbation Theory for Linear Operators. Classics in Mathematics. Springer, Berlin (1995)
19. Kurata, K., Shibata, M.: Least energy solutions to semi-linear elliptic problems on metric graphs. J. Math. Anal. Appl. **491** 124297 (22 pages) (2020)
20. Latushkin, Y., Sukhtaiev, S.: An index theorem for Schrödinger operators on metric graphs. Contemp. Math. **741**, 105–119 (2020)
21. Marzuola, J.L., Pelinovsky, D.E.: Ground state on the dumbbell graph. Appl. Math. Res. Express. AMRX **1**, 98–145 (2016)
22. Noja, D., Pelinovsky, D.E. (eds.): Symmetries of Nonlinear PDEs on Metric Graphs and Branched Networks. MDPI, Basel (2019)
23. Noja, D., Pelinovsky, D.E.: Standing waves of the quintic NLS equation on the tadpole graph. Calc. Var. Partial Differ. Equ. **59** (2020) 173 (31 pages)
24. Noja, D.: Nonlinear Schrödinger equation on graphs: recent results and open problems, Philos. Trans. R. Soc. A, **372**, 20130002 (20 pages) (2014)
25. Noja, D., Pelinovsky, D., Shaikhova, G.: Bifurcations and stability of standing waves in the nonlinear Schrödinger equation on the tadpole graph. Nonlinearity **28**, 2343–2378 (2015)
26. Shatah, J., Strauss, W.: Spectral conditions for instability, Nonlinear PDE's, dynamics and continuum physics (South Hadley, MA, 1998), Contemp. Math. Am. Math. Soc., Providence, RI, **255**, 189–198 (2000)
27. Teschl, G.: Ordinary Differential Equations and Dynamical Systems, Graduate Studies in Mathematics 140. AMS, Providence (2012)